

Experimental Investigation of a Steel-Framed Building for Disproportionate Collapse

EBIJI AKAH, CURTIS WOOD, KAI LI and HALIL SEZEN

ABSTRACT

This paper presents the experimental and numerical investigation of the progressive collapse vulnerability of an existing steel building, Haskett Hall, on the Ohio State University campus. The building was tested by removing one of the first-story columns to observe its collapse resistance and to evaluate the effectiveness of current modeling and analysis guidelines. Progressive collapse is a relatively large partial or complete collapse of a structure due to the loss of a vertical load-carrying element—a column in this case. Few researchers have been able to conduct full-scale experiments to understand the progressive collapse mechanism. In this research, deflections and deformations of steel structural components were measured during the field experiment. Computational models and simulations were examined and compared with the experimental data from the field tests. The contribution and effects of infill walls to progressive collapse resistance of frame structures were investigated. The test data collected in this research can be used to help develop recommendations for improved procedures for progressive collapse analysis of frame buildings.

Keywords: steel frame, disproportionate collapse, full-scale experiment, infill wall.

BACKGROUND INFORMATION

The term *progressive collapse* can be defined as the partial or total collapse of a structure that may be caused by local structural failure. The General Services Administration (GSA), American Society of Civil Engineers (ASCE), and the U.S. Department of Defense (DoD) have developed guidelines to evaluate, design and improve progressive collapse resistance of existing and new buildings. The GSA (2013) outlines procedures to evaluate whether a building, based on its size and shape, is vulnerable to progressive collapse. ASCE 7 (2010) and the AISC *Seismic Provisions* (AISC, 2010) both outline approaches to maintain structural integrity when a load-carrying member is damaged. Lastly, UFC 4-023-03 outlines how to prevent progressive collapse in multistory buildings (DoD, 2013). This research uses these guidelines to test and analyze whether a given structure is susceptible to progressive collapse. This paper focuses on the instrumentation and testing of Haskett Hall,

shown in Figure 1, to determine the potential for progressive collapse. One column was removed from the building within a short time period, as recommended by the GSA design guidelines, by Loewendick Demolition Contractors in November 2013. The two-dimensional (2D) linear static and nonlinear dynamic structural analyses have been performed using structural analysis programs to compare with the simulated and experimental data. This experiment is part of a larger research program at the Ohio State University (OSU) involving steel frame, reinforced concrete, and masonry buildings. (Akah, 2015; Li, 2017; Song and Sezen, 2013; Song et al., 2014)

BUILDING DESCRIPTION

Haskett Hall was a four-story building built in 1925 on the OSU campus in Columbus, Ohio. The building consisted of classrooms, offices and laboratories. A section on the north side of the building was used as a three-story testing laboratory. According to the original construction drawings provided by OSU, the building included built-up steel columns using rivets and channels, reinforced concrete slabs for the flooring, and steel I-beams encased with concrete. Figure 2 shows the elevation of the exterior frame on the west side of the building, including dimensions between centerlines of beams and columns. The building included a grid of seven columns that ran in the north-south direction and six columns that ran in the east-west direction. The total number of primary columns for the building was 38 (Figure 3). Occasionally, joists below floor slabs were used in the east-west direction. Joists were typically spaced at 2.08 ft (0.64 m). Typical reinforced concrete slab thickness was 7.0 in. (178.0 mm) without joists and 2.5 in. (63.5 mm) with joists.

Ebiji Akah, Design Engineer, SMBH Inc., Columbus, OH. Email: eakah@smbhinc.com

Curtis Wood, Senior Structural Engineer, E.L. Robinson Engineering, Columbus, OH. Email: cwood@elrobinson.com

Kai Li, Ph.D. Candidate, Department of Civil, Environmental and Geodetic Engineering, The Ohio State University, Columbus, OH. Email: li.3910@osu.edu

Halil Sezen, Professor, Department of Civil, Environmental, and Geodetic Engineering, The Ohio State University, Columbus, OH. Email: sezen.1@osu.edu (corresponding)

Paper No. 2017-04R

Historic sections and built-up column members were represented by equivalent sections in the programs (SAP2000, 2011). Properties of these sections were based on the original plans and the AISC database of historically available sections, as described earlier (Brockenbrough, 2003). When the building was designed in 1924, structural steel had to conform to the ASTM A9-21 standard, which had a minimum required tensile strength of 60,000 psi and a minimum required yield point of 30,000 psi. Yield strength for the beams and columns are assumed to be 36,000 psi, also assuming the actual yield strength would be slightly higher than the required minimum. Some of these beams were encased with concrete with a specified compressive strength of 4,000 psi. The cross-section of the encased floor beams is shown in Section G-G in Figure 4. Steel beams located in the perimeter frames were partially encased in concrete for fireproofing (Figure 5). Beams were connected to columns

using rivets through angles that were located on the bottom flanges and webs (Figure 5). The reinforced concrete slab on beams created a more rigid connection with some composite action. The primary columns within the building were built-up sections—I-sections bracketed by two channel sections that were connected with rivets (e.g., column 27 in Figure 3). The original plans did not detail specific beam types. The beam depth and weight/foot were listed as 15" I @42[#], 18" I @55[#], 24" BI @73.5[#] etc. Known beam dimensions were used to determine, for example, that the 15" I @42[#] was a B15×42. The remaining beams were not exposed during the experiment; therefore, the closest historic beams with “B” designation were chosen for consistency. If a “B” type beam was not available, “G” designated beams were used. Member selection considered historic standard sections that were available during the 1924 construction of Haskett Hall. A similar selection process was used for column sizes.



Fig. 1. Haskett Hall.

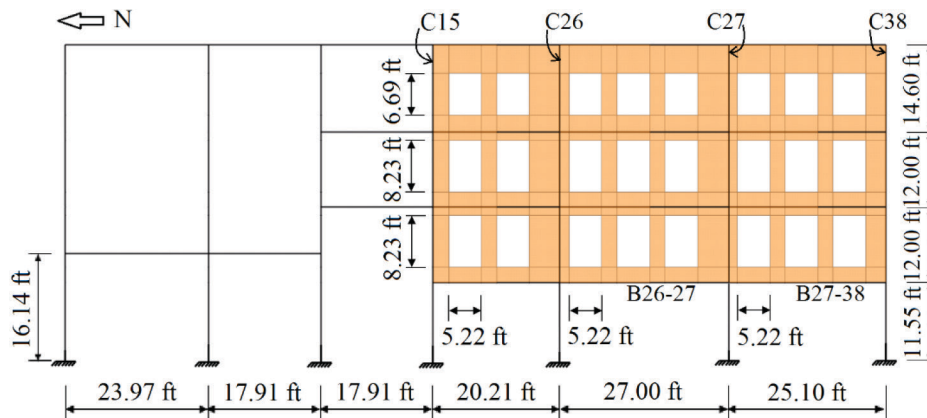


Fig. 2. Haskett Hall western elevation and bay layout.

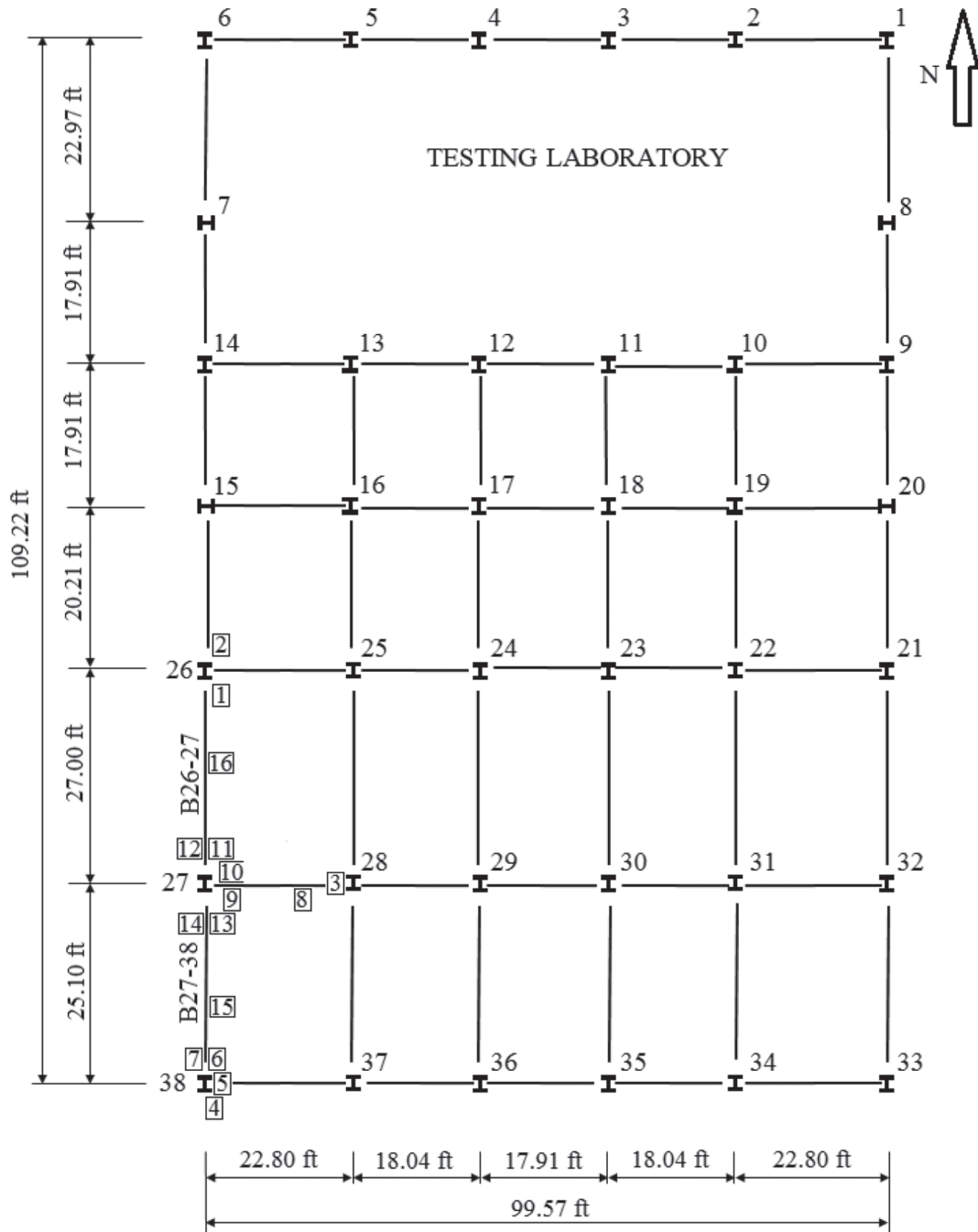


Fig. 3. Haskett Hall simplified layout with strain gauges on columns (numbered 1–7 in rectangle) and beams (8–16).

INSTRUMENTATION AND COLUMN REMOVAL

GSA (2013) specifies that buildings are analyzed for progressive collapse by removing a first-story column at the middle of the long side of the structure, the middle of the short side of the structure, and at a corner of the structure. However, after initial discussions with the demolition contractor, it became apparent that only one column would be removed by the demolition contractor structure. While not exactly in the middle of the long side of the building, column 27 (Figure 3) matched the closest to the GSA guidelines of the available columns. Column 27 was removed by the use of a processor—a hydraulic demolition shear equipment attached to a large trackhoe/excavator. The processor was placed around column 27 and a section of the column was crushed by the claws of the processor. By using the processor, column removal time was minimized. Table 1 details the column removal process.

Strain gauges, installed on three neighboring columns and three connecting beams, measured uniaxial strains during the column removal. Furthermore, linear variable differential transformer displacement sensors (LVDT) measured the vertical and horizontal vibrations and displacements around the removed column. A total of 16 strain gauges were used in the experiment: seven were attached to columns and nine were attached to beams. Columns 26, 27 and 38, along with the adjoining first-story beams, were exposed and cleaned for strain gauge attachment. Because Haskett Hall was a steel-framed building, only the brick façade and exterior infill walls were required to be removed. All interior dry-wall had previously been removed. The strain gauges were installed on both the flanges and the webs of the neighboring columns. All beams had gauges placed on the bottom face

of the bottom flange. Column 26 had two gauges installed 3.08 ft from the base of the column. Column 38 had three gauges installed 6.17 ft from the base and one gauge 4.58 ft from the base. Column 28 had one gauge placed 4.58 ft from the base. Three LVDT or displacement sensors were used in Haskett Hall. Two LVDT were placed vertically on both side of column 27 and one LVDT was placed horizontally at the beam-column joint. Figures 3 and 6 show strain gauge and LVDT placement.

Fifteen strain gauges recorded dynamic strain data during column removal. There were five distinct physical events, and the corresponding measured strain histories helped understand the behavior of the building during those events. Initially, all strain gauges and displacement sensors had stable readings. When the processor made contact with the test column, strain and displacement values started to increase. A period for the processor began when the claw closed, making contact with the column (Figure 7, left), and ended when the claw opened and was no longer in contact with the column (Figure 7, right). These five periods are shown in Table 1. Figure 8 shows column 27 (in red circle) that was scheduled to be demolished before removal (top) and after removal (bottom).

Analysis of Measured Strains

The measured strains captured the effects of the processor movements and helped understand the response at the strain gauge locations. Figure 8 shows strain histories measured by strain gauges 1–7. It presents how the processor's contact with the column affected the measured strain values. At each time that the processor made contact with the removed column, there was a jump in the measured strain.

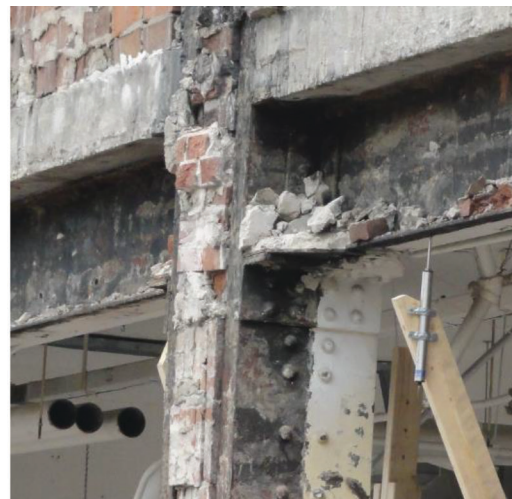
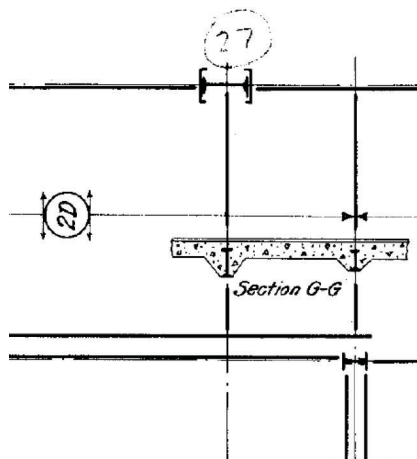


Fig. 4. Close-up detail of column 27 encased in concrete (partial plan view from original drawings), and beam-column connection with rivets through angle on beam bottom flange and web.

Table 1. Processor Contact with Test Column

Contact Number and Event	Contact Start Time, sec	Contact End Time, sec
1. Strains/displacements increased from zero	168.5	177.7
2. Bricks in exterior column web crumbled	184.6	191.2
3. Column bent inward	208.6	218.5
4. Column warped and twisted by processor	221.6	231.8
5. Column was cut through and second floor beams deflected downward	247.8	251.7



Fig. 6. Vertical LVDT to the south (in circle on left) and north (in circle on right) of the removed column and horizontal LVDT (rectangle) attached to the removed column.



Fig. 7. Column 27 under removal (left) and finished removal (right).

With strain gauge 3, the first contact time started at 168.49 seconds, with the processor closing its claw, and resulted in a strain increase of approximately -20×10^{-6} in./in. Negative strain values indicate compression and positive strain values indicate tension. Once the processor opened its claw and was no longer in contact with the column at a time of 177.65 seconds, the strain fell to -15×10^{-6} in./in. This overall decrease in strain exhibits the change, and overall increase, in axial compressive load on column 28. The same effect is apparent from when the processor closed and opened its claw three more times: from 184.61 to 191.17 seconds, 208.62 to 218.54 seconds, and 221.60 to 231.76 seconds. During these contact times, the column's inserted bricks began to crumble, the column became bent inward and started to become warped by the processor's twisting.

During the last processor contact time, which lasted from 247.77 to 251.74 seconds, the test column was completely cut through, and the connecting beams deflected downward.

It should be noted that the test column was cut by altering the position of the processor, meaning there was a three-dimensional cutting plane. In Figure 9, once the column was cut, the measured strain value drastically increased momentarily. Once the processor was no longer in contact with the cut column, the measured strain leveled out at approximately -29×10^{-6} in./in for strain gauge 3. Assuming the steel did not yield, the compressive axial stress increase, Δf , on the east side of column 28 was approximately 0.9 ksi—that is, $\Delta f = E_s \epsilon_s = (29,000 \text{ ksi})(29 \times 10^{-6} \text{ in./in.})$.

Table 2 shows that each strain gauge located on a column measured a residual negative strain value, indicating that each column neighboring the removed column underwent compression once the test column was removed. The south column 38, which measured the largest negative residual strain, had to carry more additional axial force than the east column 28 or north column 26. Furthermore, the magnitude of strain values on the columns increased from south to



Fig. 8. Penultimate column 27 before removal (top) and after removal (bottom).

Table 2: Strain Values Measured at 300 Sec by Strain Gauges on Columns

Gauge No.	Column	Location	Height on Column, ft	Strain, $\times 10^{-6}$ in./in.
1	26	South flange	3.08	-32
2	26	North flange	3.08	-54
3	28	West web	4.59	-29
4	38	South flange	6.17	-7
5	38	East web	6.17	-61
6	38	North flange	6.17	-103
7	38	North flange	4.59	-93

north and west to east, exhibiting that some limited the axial loads were being transferred into the building column 28 and 38.

Measured Displacements

Three displacement sensors recorded dynamic displacements during the column removal. When the processor made contact with the test column at 169 seconds, displacement values started to increase (Figure 10). The five times the processor made contact with the column are described in Table 1. Dynamic measurements of displacement that appear after 300 sec in Figure 11 were a result of the processor making contact with the test column, but for the sake of the experiment, data measurements were meant to be terminated once the column was completely removed shortly after 250 sec. The measured displacement data were compared with results from the structural analysis models. For

the purpose of presenting data clearly and straightforward, the vertical displacement scales of Figures 10 and 11 are different by a factor of 10.

STRUCTURAL MODELING AND ANALYSIS

Two-dimensional linear static (2D LS) and nonlinear dynamic (NLD) structural analyses of the western frame of Haskett Hall were performed in SAP2000 (2011). A critical modeling question is whether the steel beams behaved compositely with the concrete deck. Shear studs or other means of connection between the beams and slab were not used during construction of Haskett Hall. However, the beams were embedded into the concrete, as seen in Figures 4 and 5(b). In some instances, the concrete even extended the entire depth of the web. For structural analysis, it would be conservative to assume noncomposite behavior. However, this assumption may not yield results consistent with the field testing.

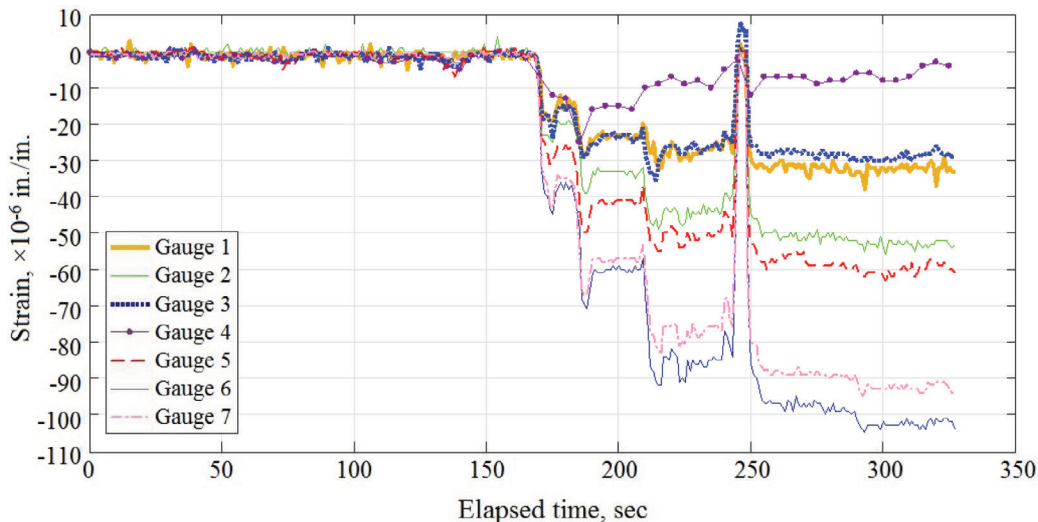


Fig. 9. Strain history measured by strain gauges 1–7 on steel columns.

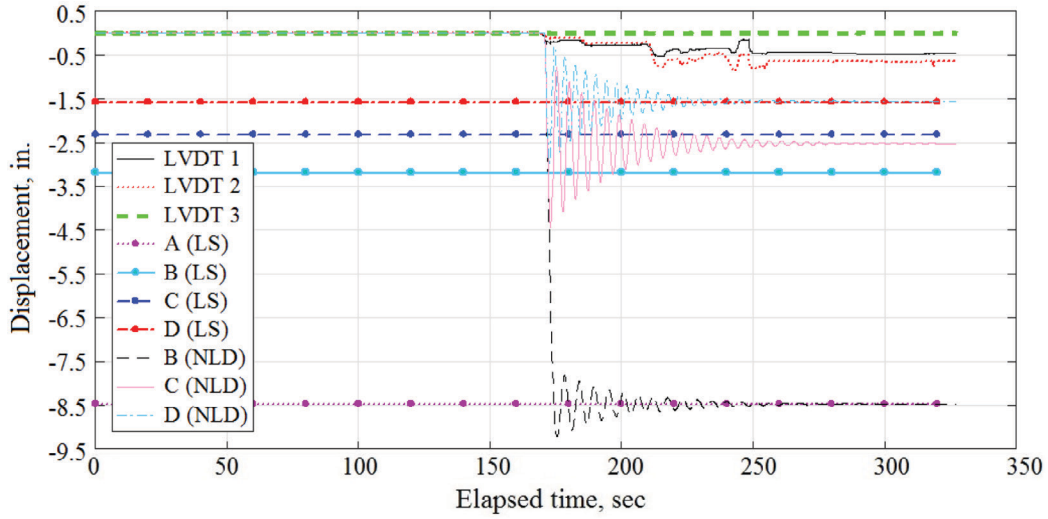


Fig. 10. Comparison of measured LVDT deflections to linear static (LS) and nonlinear dynamic (NLD) calculated deflections of models: A (noncomposite beam, no slab in upper floors); B (composite beams, no slab in upper floors); C (noncomposite beams and ribbed slabs in upper floors); D (composite beams and ribbed slabs in upper floors).

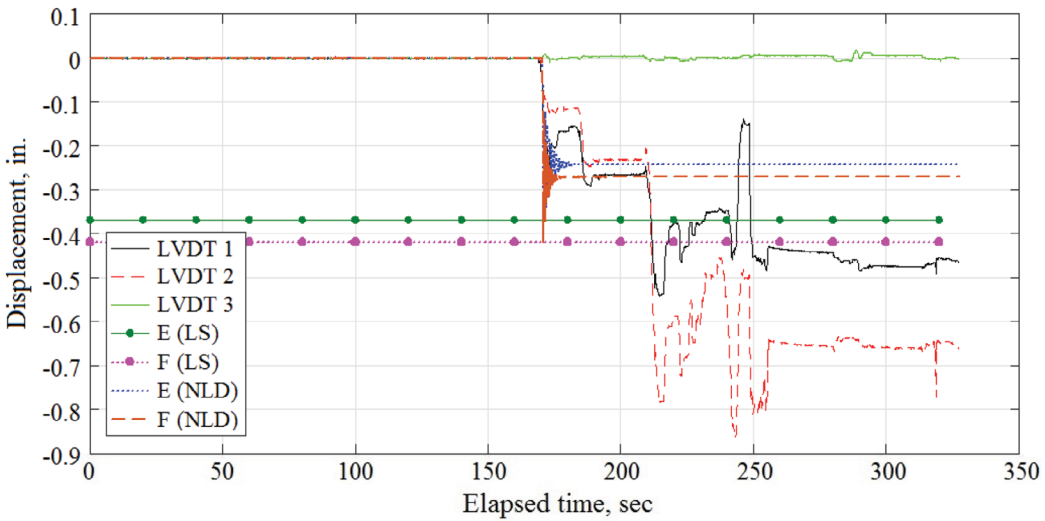


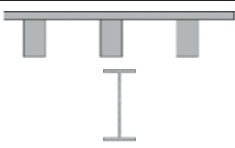
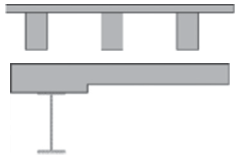
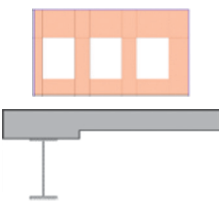
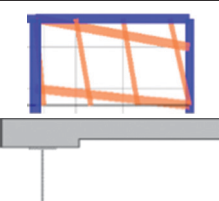


Fig. 11. Comparison of measured LVDT deflections to linear static (LS) and nonlinear dynamic (NLD) calculated deflections of models: E (composite beams and shell elements for infill walls); F (composite beams and tension-only strut elements for infill walls).

Table 3. Calculated Deflections at Top of Column 27 with Different Modeling Assumptions

Model	Model Assumptions	Model Details	Linear Static, in.	Change against Test Result	Nonlinear Dynamic, in.	Change against Test Result
A	Noncomposite beam, no slab in upper floors		8.46	1165%	Failed	N/A
B	Composite beams, no slab in upper floors		3.19	376%	8.47	1165%
C	Noncomposite beams, and ribbed slabs in upper floors		2.32	246%	2.52	276%
D	Composite beams, and ribbed slabs in upper floors		1.57	135%	1.56	133%
E	Composite beams and shell element for infill walls		0.37	-45%	0.24	-64%
F	Composite beams and tension-only strut elements for infill walls		0.42	-37%	0.27	-60%

Another nontypical detail in Haskett Hall was the ribbed slabs on the third and fourth floors. The ribbed slab consisted of multiple, small transverse concrete ribs below the slab. The ribbed slabs spanned between the steel beams. These slabs did not include an edge beam but were embedded into the façade at the end, as seen in Figure 5(c). This presented difficulty when developing the 2D model of the perimeter frame. Because there was not an actual beam to model, an assumption was made to include the portion of ribbed slab in the upper floors equivalent to the effective width in the composite beam-slab sections on the lower floors. The 2D perimeter frame was modeled using both composite and noncomposite beams. As shown in Table 3, four different assumptions were considered: noncomposite beams in the lower floors and no beams or slabs in the upper floors (model A), composite beams and no ribbed slabs in upper floors (model B), noncomposite beams in lower floors and

ribbed slabs in upper floors (model C), and composite beams and ribbed slabs in upper floors (model D). The maximum calculated deflections of models were compared with the experimental deflections in Table 3. The average experimental or measured maximum displacement on top of the removed column (column 27) was 0.67 in. The inclusion of the ribbed slab sections significantly influenced the overall behavior of the structure. The composite beam and ribbed slab model (model D) yielded the closest response to the experimental results for both the linear static analysis and nonlinear dynamic analysis (Table 3 and Figure 9).

Axial Load Distributions

The behavior of noncomposite and composite beam models were further compared through calculated axial load and moment distributions. Axial load distributions before and

Model	Test Column Pre-Removal, kips	Pre-Removal, kips		Post-Removal, kips		Change in Axial Force, kips		Total Change in Axial Force, kips	Increase in Axial Force, kips
	C27	C26	C38	C26	C38	C26	C38	C26 + C38	C26 + C38 over C27
A	145.5	126.1	77.8	192.2	160.1	66.1	82.3	148.4	2.0%
B	146.4	127.2	76.9	203.9	154.0	76.7	77.1	153.8	5.1%
C	146.8	123.2	76.4	192.2	154.9	69.0	78.5	147.5	0.5%
D	147.7	124.3	75.8	196.7	153.3	72.4	77.6	150.0	1.6%

after removal of the test column C27 for models B and C are shown in Figures 12 through 15. When compared with the calculated axial load in the test column (C27), the ribbed slab models (models C and D in Table 3) have the lowest total change in axial force in neighboring columns C26 and C38—that is, an increase of 0.3% and 1.7%, respectively, in Table 4. As the composite action increases, the total change in axial forces in columns C26 and C38 also increases compared with the test column C27. Specifically, in the non-composite beam model without ribbed slabs (model A), axial forces increase by 2.0%, while in the composite without ribbed slabs (model B), axial forces increase by 5.1%. Comparison of axial forces between the models with and without ribbed slabs show that in the models with ribbed slabs, larger axial forces are transferred to the neighboring columns (C26 and C38).

Moment Distributions

The maximum moments calculated from linear static analysis after removal of critical beams from the models. The unfactored demand-capacity ratios for plastic moments (DCR_p) are shown in Table 5. The unfactored load is the

load combination with no live load and dead load factored by 1.0. DCR_p is defined as the ratio of calculated maximum moment in a member to its plastic moment capacity, $M_p = F_y Z$, where F_y is yield strength and Z is the plastic section modulus. After column removal, the calculated maximum moments are larger in magnitude for models without ribbed slabs (models A and B) when compared with the models with ribbed slabs (models C and D). This shows that for both cases, the moments in beams in lower floors increase when the ribbed slabs are neglected and that the ribbed slab contributes to load redistribution. Comparison of calculated beam moments with flexural limits shows that the composite action generally led to a decrease in the unfactored DCR_p by increasing the flexural strength. For example, the DCR_p for models without ribbed slabs, beam B27-38 (Figure 2) had a DCR_p of 2.46 and 0.90 in models A and B, respectively. For models with ribbed slabs, the DCR_p for beam B27-38 is 0.88 and 0.49 in models C and D, respectively. In general, models with ribbed slabs have a lower DCR , showing that the ribbed slabs increase the overall flexural resistance of the frame. Moment diagrams before and after removing the test column C27 for model C are shown in Figures 16 and 17, respectively.



Fig. 12. Calculated axial load distribution for model B (with composite beams and no ribbed slabs) before the test column removal (under red cross).

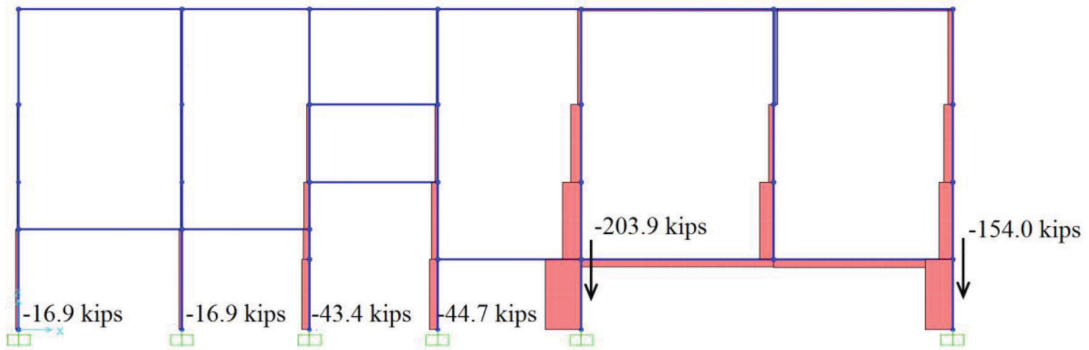


Fig. 13. Calculated axial load distribution for model B (with composite beams and no ribbed slabs) after the test column removal.

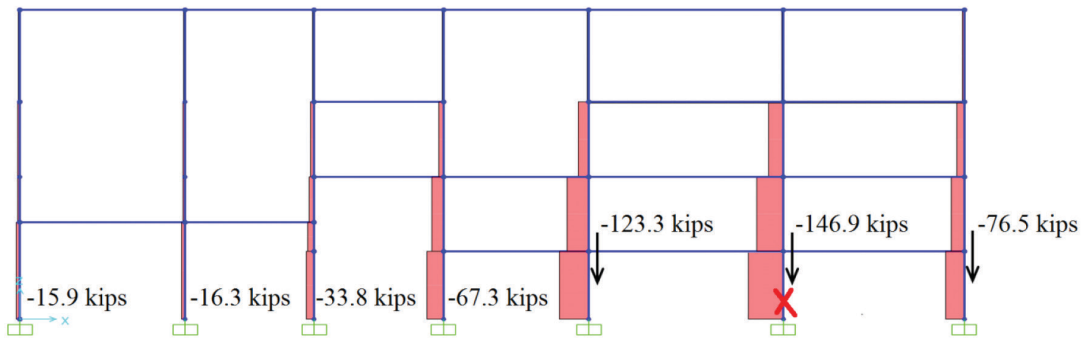


Fig.14. Calculated axial load distribution for model C (with noncomposite beams and ribbed slabs) before the test column removal (under red cross).

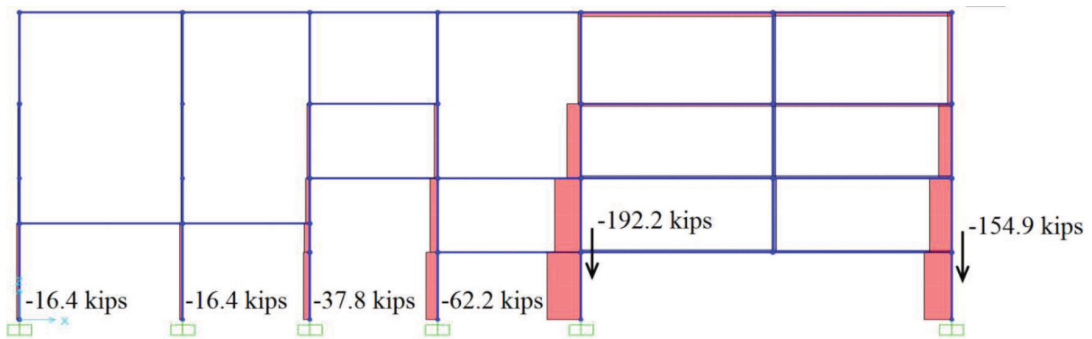


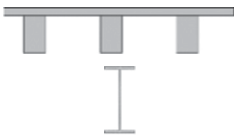
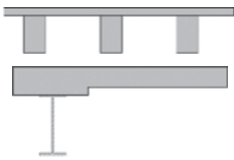
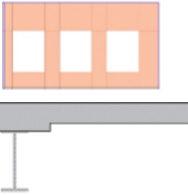
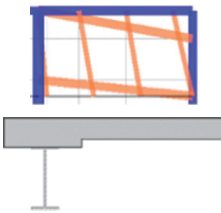


Fig. 15. Calculated axial load distribution for model C (with noncomposite beams and ribbed slabs) after the test column removal.

Table 5. Unfactored DCR of Connecting Beams (M_{max}/M_p)

Model	Model Detail	Model Detail Figures	DCR _p	
			B (26-27)	B (27-38)
A	Noncomposite beam, no slab in upper floors		2.34	2.46
B	Composite beams, no slab in upper floors		0.95	0.90
C	Noncomposite beams, and ribbed slabs in upper floors		0.92	0.88
D	Composite beams, and ribbed slabs in upper floors		0.54	0.49
E	Composite beams and shell element for infill walls		0.21	0.13
F	Composite beams and compression-only strut elements for infill walls		0.38	0.39

INFILL WALL CONTRIBUTION

During the field experiment, the perimeter frame of the Haskett Hall was partially filled with unreinforced masonry walls at the second to fourth floors between the axis of 15 and 38 (Figure 1 and 2). The infill walls were directly attached to the structural beams and columns. Masonry walls have low tension strength but can provide additional stiffness in compression. As a result, it is expected that the infill walls will increase the progressive collapse resistance of Haskett Hall.

Infill walls had two types of window openings: 8.23 ft by 5.22 ft and 6.69 ft by 5.22 ft openings in the second and third stories (Figure 2). Figure 4 shows the cross-section cut through the window openings and indicates that only half of

the infill wall sits on the structural floor slabs. Therefore, in the SAP2000 model, only half of the original 12-in. thickness of the infill masonry wall was modeled. The default lower bound compressive strength of the masonry material, f'_m , was assumed to be 600 psi, as defined in ASCE 41-13 (2013). The expected strength, f_{me} , of 780 psi is used in this research (a factor of 1.3 is used to translate lower bound property to expected masonry property).

The second and third floor slabs modeled as ribbed slabs were simplified as a rectangular concrete beam of a 6.5-in. by 2-in. cross section. The infill walls were modeled using shell elements and equivalent strut elements. The shell elements with four nodes are used to model infill walls with window openings. In the equivalent strut method, the elastic in-plane stiffness of a solid unreinforced masonry wall

before cracking was modeled as an equivalent diagonal compression strut. For each strut, the elastic modulus was calculated from Equation 1 (Shames and Cozzarelli, 1997).

$$E_{\theta} = \frac{1}{\frac{1}{E_0} \cos^4 \theta + \left(-\frac{2\nu_{0-90}}{E_0} + \frac{1}{G} \right) \cos^2 \theta \sin^2 \theta + \frac{1}{E_{90}} \sin^4 \theta} \quad (1)$$

where θ is the angle whose tangent is the infill height-to-length aspect ratio; E_0 and E_{90} are the Young's modulus in the direction parallel and normal to the bed joints, respectively; ν_{0-90} is the Poisson's ratio; and G is the shear modulus. According to TMS (2011), $E_{90} = 900f'_{m-90}$, in which f'_{m-90} represents the expected compressive strength normal to the bed joint. $E_0 = 0.7E_{90}$, and $G = 0.4E_{90}$.

According to ASCE 41-13 (2013), the equivalent compression strut analogy shall be used to represent the elastic stiffness of the unreinforced masonry infill masonry wall of width a , given by Equation 2.

$$a = 0.175(\lambda_1 h_{col})^{-0.4} r_{inf} \quad (2)$$

in which

$$\lambda_1 = \left[\frac{E_{\theta} t_{inf} \sin 2\theta}{4E_{fe} I_{col} h_{inf}} \right]^{1/4} \quad (3)$$

where h_{col} is the column height between the centerlines of beams above and below the columns; r_{inf} and t_{inf} are the diagonal length of infill panel and thickness of infill panel, respectively; E_{fe} is the expected modulus of elasticity of the bare frame material; I_{col} is the moment of inertia of the column; h_{inf} is the height of infill panel; and E_{θ} represents the adjusted elastic modulus of the infill masonry material, which is calculated from Equation 1.

The infill walls are modeled by using two equivalent diagonal struts connected to the structural frame elements. ASCE 41-13 indicates that the tensile strength of masonry is only 10 psi for the fair condition, which is only one-sixtieth of its compressive strength, 600 psi under the same condition. For the poor stage of the unreinforced masonry, tensile strength is evaluated even as 0 psi. Due to the long-time use of Haskett Hall from its construction in 1925, the masonry

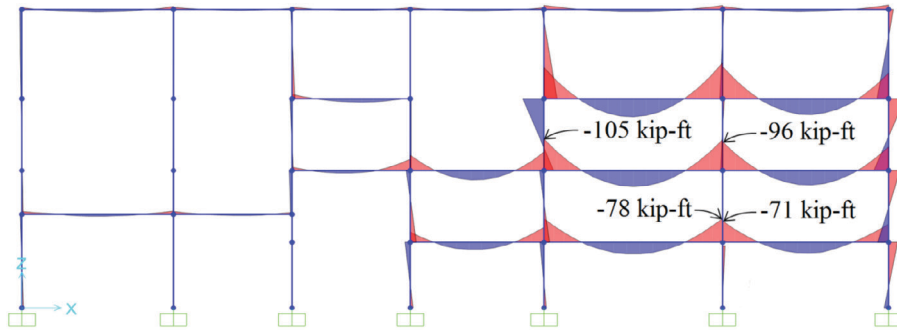


Fig. 16. Moment diagram for noncomposite with ribbed slab model (C) before test column (circled) removal. Values are for maximum moment demands in beams.

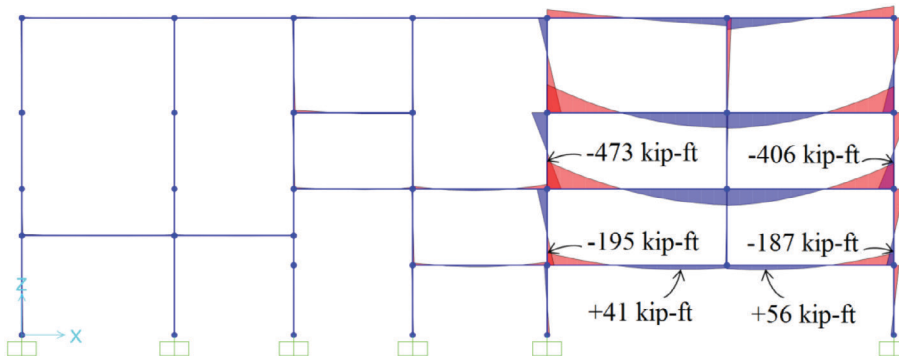


Fig. 17. Moment diagram for noncomposite with ribbed slab (C) model after test column removal. Values are for maximum moment demands in beams.

walls are likely to have potential material deficiencies and weakness between the mortar and red brick units. In this research, tensile strength of the unreinforced masonry is modeled as 0 psi. Based on this assumption, all struts subjected to tensile forces are supposed to be removed from the model. To achieve this goal in SAP2000 analysis, tension and compression stress distribution patterns of shell elements are obtained firstly as shown in Figure 18. The compression arrows are marked in warm colors (negative values), and tension arrows are marked in cold colors (positive values) on each shell element. A couple of arrows of each shell element are sustained tensile strengths and compression strengths, respectively, in the orthogonal direction. In the strut element method, the stress arrows can be roughly replaced by struts because the compressive and tensile strength are ultimately transferred to structural elements, and the struts are

connected with structural components as well. By identifying the tension strength strut from the stress pattern diagram, one of the couple diagonal struts in the diagonal section is removed from the strut element model. The compression-only strut element model is developed and presented in Figure 19. All the struts were developed as frame elements with very large moment of inertia to act as truss members with axial deformation and strength only.

The shell element infill wall model is labeled as model E, as shown in Figure 18, and the compression-only strut element infill wall model is marked as model F (Figure 19). The linear static (LS) and nonlinear dynamic (NLD) analyses of infilled steel structure were performed and generated the 2D deflection data in Table 3. By comparison with the deflection data of all four bare steel structure models, the results of infilled steel structure models are much closer to the field

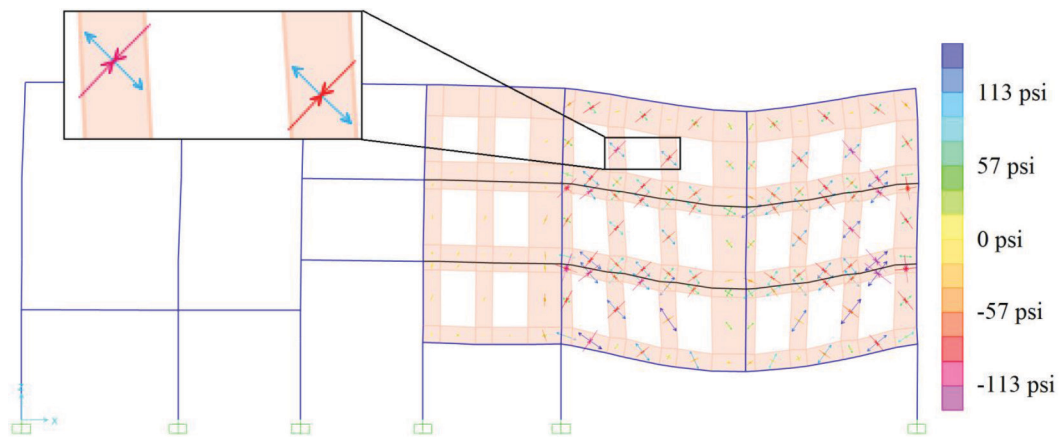


Fig. 18. Maximum stress distribution in model E with infill wall shell elements (and ribbed slabs in upper floors) after test column removal.

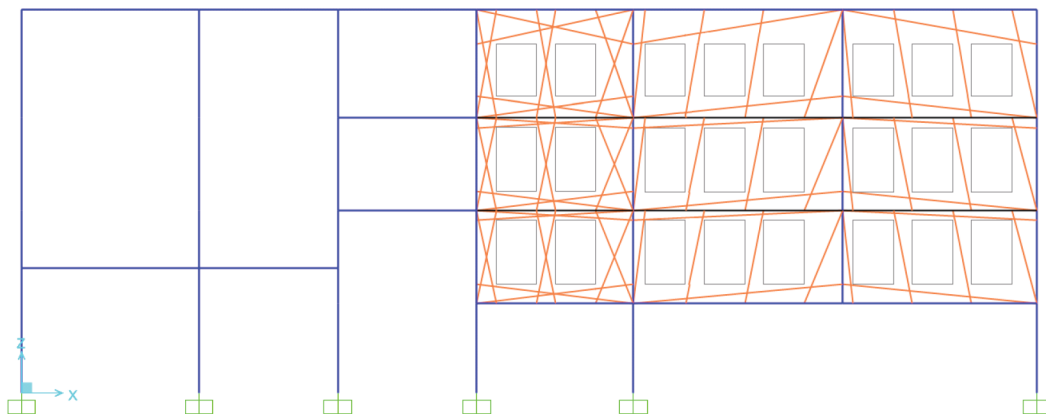


Fig. 19. Haskett House frame structure with compressive strut elements for representing infill walls.

test of Haskett Hall. Both LS and NLD analyses of model E and F yielded a maximum 64% difference ratio compared with experimental data, while the bare frame models A through D developed differences more than 100%, which indicates that the stiffness of masonry infill walls connected to the steel structural elements plays an important role in progressive collapse resistance. The infilled frame structure model was proved to decrease a minimum of 20.4% in DCR_p and increase the elastic stiffness 57.6% compared with bare frame structure model.

The calculated outcomes of two infill wall frame models E and F were compared with the measured LVDT deflections in Figure 10. It is clearly shown that the results from both the shell element model and the strut element model have higher agreement on the field test results than that of bare frame models A through D. The masonry infill walls can be simply modeled using equivalent strut element. Moreover, the strut element approach was better at modeling the unreinforced masonry wall because shell elements cannot identify and remove the tensile strength members. Figure 10 shows that both the linear static and nonlinear dynamic analyses results from strut element model F are closer to the field test data than that of shell element model E. More tensile strength contributions are made from shell elements; however, unreinforced masonry wall have little tension capacity.

Based on Figure 18, the stress distribution diagram of the infill walls is presented. It is observed that the large-magnitude stresses distribute on the infill walls of the bays in which the column was removed—that is, between axes 26 and 38. Lesser-magnitude stresses are distributed on the infill walls between axes 15 and 26. It indicates that only the infill walls within the bays where structural frames were removed develop compression and tension stresses. In general, the stiffness contribution of the masonry infill wall will be considered when large deformation appears in its attached structural frames. In Haskett Hall, large displacement was observed at column 27. The infill walls between C26 and C27 and C27 and C38 were under significant stresses and contributed in progressive collapse resistance. The DCR_p of the infill wall frame models are shown in Table 5. The maximum DCR_p of infill wall models is 0.39, which is smaller than the DCR_p of all the bare frame models. The comparison shows that the infill walls increase the flexural resistance of the steel structural frame and decrease the progressive collapse probability.

CONCLUSIONS

Haskett Hall was designed and completed in the 1920s, utilizing unique, as well as outdated, design methods. Full-scale experimental data were obtained during the removal of a first-story column. This unique field experiment on the perimeter frame of a steel building and numerical analyses have shown that the internal forces, including the axial

load, on a first-story column is mainly transferred to the two neighboring columns without collapse. Due to lack of such full-scale building test data, the data measured in this research have been an invaluable addition to the state of knowledge on gravity collapse of actual buildings.

Two-dimensional linear static and nonlinear dynamic analysis results of four types of bare-frame models were compared with the data measured in the field. Analyzing the experimental and theoretical responses of the two-dimensional frame, the numerical calculation results exceeded the field data for linear static analysis and underestimated the results for nonlinear dynamic analysis. Including the ribbed slab sections appears to be critical to accurately capture the true behavior of the structure. The appropriate width of the ribbed slab to include on a two-dimensional analysis needs to be further researched. The infill wall model E shell element and the model F compression-only strut model improved the Hasket Hall structural modeling by yielding closer results to the field test data. By using the compression-strut element approach to model the unreinforced masonry infill wall, analysis results exhibited a high agreement with the field test results. It is concluded that the infill wall can improve the progressive collapse resistance performance by stiffening the structure and dissipating energy in smaller deformation. The infill walls within the column loss area can improve the stiffness of the structure as the large deformations appear.

ACKNOWLEDGMENTS

This research project is partially supported by the American Institute of Steel Construction (AISC) and the National Science Foundation (CMMI 1130397 and 1435446). The authors would like to thank the Loewendick Demolition Company and the Office of Facilities Operations and Development at the Ohio State University for providing the original building drawings. M. Lodhi, J. Wade and N. Savage helped with the experiment and initial member size data interpretation in SAP2000. The AISC research director, Tom Schlafly, observed the testing of Haskett Hall. This technical assistance and financial support are greatly appreciated. Opinions, findings and conclusions are those of the writers and do not necessarily reflect those of the sponsoring agencies.

REFERENCES

- Akah, A. (2015), *Experimental and Analytical Collapse Evaluation of an Existing Building*, M.S. Thesis, The Ohio State University, Columbus, OH.
- AISC (2010), *Seismic Provisions for Structural Steel Buildings*, ANSI/AISC 341-10, American Institute of Steel Construction, Chicago, IL.
- AISC (2011), *Steel Construction Manual*, 14th ed., American Institute of Steel Construction, Chicago, IL.

- ASCE (2010), *Minimum Design Loads for Buildings and Other Structures*, ASCE 7-10, American Society of Civil Engineers, Reston, VA.
- ASCE (2013), *Seismic Rehabilitation of Existing Buildings*, ASCE 41-13, American Society of Civil Engineers, Reston, VA.
- Brockenbrough, R. (2003), *Rehabilitation and Retrofit Guide—A Reference for Historic Shapes and Specifications*, Design Guide 15, American Institute of Steel Construction, Chicago, IL.
- DoD (2013), *Design of Buildings to Resist Progressive Collapse*, UFC 4-023-03, Department of Defense, Arlington, VA.
- GSA (2013), *Progressive Collapse Analysis and Design Guidelines for New Federal Office Buildings and Major Modernization Projects*, General Services Administration, Washington, DC.
- Li, K. (2017), *Collapse Assessment of Buildings by Wall Removal and Vision-Based Measurement Applications*, Ph.D. Dissertation, The Ohio State University, Columbus, OH.
- SAP2000 (2011), *SAP 2000 Advanced Structural Analysis Program*, Version 15.1, Computers and Structures Inc., Berkeley, CA.
- Shames, I.H. and Cozzarelli, F.A. (1997), *Elastic and Inelastic Stress Analysis*, Taylor & Francis Ltd, Philadelphia, PA.
- Song, B., Giriunas, K. and Sezen, H. (2014), “Progressive Collapse Testing and Analysis of a Steel Frame Building,” *Journal of Constructional Steel Research*, Vol. 94, pp. 76–83.
- Song, B. and Sezen, H. (2013), “Experimental and Analytical Progressive Collapse Assessment of a Steel Frame Building,” *Engineering Structures*, Vol. 56, pp. 664–672.
- TMS (2011), *Building Code Requirement for Masonry Structures and Specification for Masonry Structures and Companion Commentaries*, The Masonry Society, Longmont, CO.

